Real-Time Fault Detection and Diagnosis for Oil Well Drilling Using a Multitask Neural Network

Marios Gkionis¹ Ole Morten Aamo¹ and Ulf Jakob Flø Aarsnes² oc

¹Department of Engineering Cybernetics, Norwegian University of Science and Technology, Trondheim, Norway

²Energy Modelling and Automation, NORCE Energy, Oslo, Norway

Keywords: Fault Detection, Fault Diagnosis, Deep Neural Networks, Multitask Learning, Oil Well Drilling.

Abstract:

Drilling operations can be unexpectedly laden with mechanical faults, mud loss, and insufficient cuttings transport that incur substantial costs. This can be avoided via accurate and early fault detection and diagnosis. We present a novel Drilling Fault Detection and Diagnosis (FDD) system that leverages Multitask Neural Networks (MTL-NNs). It accounts for the practical limitation that down-hole measurements are normally not available in real-time and can perform FDD relying only on flow and pressure measurements at the drilling rig. Data for training and testing are produced by a simulator based on the distributed flow and pressure dynamics in the entire well governed by four coupled hyperbolic partial differential equations. Faults are incorporated into the simulations so that the data contain information about how diagnostics of faults affect the dynamics. Our numerical experiments, admittedly under quite ideal conditions, show that the proposed method exhibits high generalization performance on diagnosis for fixed well depths, while incorporating varying well depths into a single network requires increased size in both network and training data to maintain performance.

1 INTRODUCTION

Detection of the presence of a system fault, localization and quantification constitute the field of engineering known as Fault Detection and Diagnosis (FDD). Numerous techniques have been developed in this field (Isermann, 2006), and they can be categorized as data-based or model-based. The former (Venkatasubramanian et al., 2003) utilize historic process knowledge such as datasets from already occurred faults that can help with detection and prognosis of future faults. Rich historic datasets for faulty cases in drilling are absent, since each new well corresponds to a new (unseen) process. In addition, collecting faulty data (on purpose) would be an unrealistically expensive and lengthy process, probably making model-based methods the more feasible option for FDD in drilling. A common instance in the list of model-based FDD methods is the design of a bank of observers (Zhang, 2000), which can be based on Kalman filters, such as in (Jiang et al., 2020). Separate models are deployed for incorporation of the individual faults. Each observer corresponds to a model and is designed such that the process states and outputs are estimated and predicted respectively. The output prediction errors (residuals) are stored for statistical change analysis, thereby providing fault detection and identification. Methodical design of the statistical change detection algorithm and the observers is required and a notable example of this method applied to drilling can be found in (Willersrud et al., 2015) using down-hole measurements. However, down-hole measurements are normally not available in real-time in practice, so in the present work we rely only on *top-side measure-ments*.

Deep Learning (DL) has received rapidly increasing attention from researchers and engineers since massive amounts of data from processes are collected and create the opportunity of insight from their systematic analysis and computational tools have been improving. The enhancement of the capabilities of DL has brought about the increase in prediction accuracy, realization of explainability, and savings in training time and utilization of memory (Alzubaidi et al., 2021). In addition, two methods that help enhance generalization performance and data efficiency are MTL and Physics-Informed NNs (PINNs) (Raissi et al., 2019). The latter do so by employing math-

^a https://orcid.org/0009-0009-2626-9378

b https://orcid.org/0000-0001-6899-1451

^c https://orcid.org/0000-0001-6272-7203

ematical models that encode constitutive (physical) laws (*physics priors*) that describe the available data, which are normally either combined with the physics priors, or the priors can fully replace the data. The latter option may be desirable in applications such as drilling, given the absence of historic field data.

MTL-NNs (Caruana, 1997) are NN variants which are simultaneously trained for multiple separate prediction tasks, parameterized by shared and task-specialized parameters. Since it is a Deep Neural Network (DNN), its utilization does not come with the requirement of convergence analysis and investigation of appropriateness as a parameter estimation scheme. This requirement relaxation renders the implementation quicker and less application-specific. Up to our knowledge, MTL is at an early stage of incorporation on FDD problems. The majority of published work focuses on bearings (such as (Guo et al., 2020), (Liu et al., 2021), and (Wang et al., 2022)) and wind turbine fault diagnosis.

FDD for Drilling is fundamentally different than FDD for the aforementioned applications. In Drilling, faulty data for a new well being drilled are not available and historical data are not expected to be sufficient for DNN training and Transfer-Learning to a new well. In rolling bearing FDD, rich operation data can be utilized to extract accurate fault signatures. What is more, numerous sensors can be placed in different locations in rotary machinery applications to extract data, whereas in our case we aim to achieve FDD only using three time-series signal inputs, one of which is a manipulated signal. The current work serves as a starting point for investigating the application of MTL for FDD in drilling.

In many applications, data is available from sources that are described by inter-related latent mechanisms. Such mechanisms can be encoded through the shared part of a MTL-NN. To independently train individual NNs for each task would lead to redundant calculations of forward passes of the shared features and failure to encode the common features, thus leading to poorer generalization and parameter efficiency. The work in (Wang et al., 2021a) exemplifies this, wherein the rolling bearing vibration signals are considered in the training of the common NN, leading to the enrichment of the encoded information in the shared features. In general, learning performance can be improved when auxiliary tasks are incorporated into the NN, such as with the case of (Amyar et al., 2020) that uses the COVID classification task to enhance the learning performance of the other (main) tasks. MTL can also be valuable when sensor data are not sufficient for effective Single Task Learning (STL), as highlighted in (Wang et al.,

2021a). Among the different MTL architectures, we employ the *Multi-Head* architecture (MH-NN), which belong to the *Hard-Parameter Sharing* class of MTL architectures (Yu et al., 2024).

It has been stressed in the literature that MH-NNs are suitable for *meta-learning* (Hospedales et al., 2020). For example, the work of (Wang et al., 2021b) analyzes the connection between meta-learning and MTL through MH-NNs. In (Zou and Karniadakis, 2023), successful few-shot learning is achieved through deployment of MH-NNs, providing the first empirical observation of synergistic learning. (Lin et al., 2021) showed that MH-NNs can perform task-specific adaptation as well. This is a key motivation for opting to utilize MH-NNs in our pipeline.

In this work, the training data is generated using a transient drilling hydraulics model described by a system of four first order semilinear partial differential equations (PDEs). Despite the fact that this clearly encodes the physics of the process into the NN, it is not strictly a PINN, given that the latter utilizes the operator terms of the underlying physical laws in the NN's loss function (Raissi et al., 2019). It represents a step further from our work in (Gkionis et al., 2025), wherein a steady-state model was utilized instead. The MTL-NN approach is similar to the model-based approach, since each fault requires a separate model for data generation. Given that the NN encodes the shared feature representations, faultindependent observer design is redundant. Moreover, the NN inherently incorporates and learns the statistical assessment of residuals in the case of the design bank of observers. We examined three different flowrelated faults, which are detailed at the beginning of Section 3.

There are a few publications on Drilling FDD that utilize MTL and PINNs, albeit not referenced in analytical overviews of NN variants and FDD applications such as (Qiu et al., 2023). For instance, Convolutional NNs are applied in (Jeong et al., 2020) and (Jan et al., 2022), since the faults are provided as inputs in the form of multi-channel time series. However, these works solely examine Washout Fault Detection and up to our knowledge constitute the only ones that apply PINNs and MTL in Drilling. In (Jan et al., 2022), the different tasks include a classification task and the enforcement of physical constraints. However, the physics prior used in the estimation is tied to a specific parametric model, which restricts the generality of the NN.

We have outlined the rest of this publication as follows: Section 2 describes the pipeline of the FDD scheme; the data collection, the formulation of the data-source, and the structure and loss functions of the NN. Section 3 describes the relevant physics of the application under study and declares which exact signals are to represent the generic signals defined in Section 2. We discuss the results in Section 4 and conclude with ideas for extending the scope of this work in Section 5.

2 PROBLEM STATEMENT AND METHODOLOGY

We consider a construction task that is scheduled to be set into operation some time in the future. It is assumed to be unique, so that there is no experienced data available to learn from prior to the operation. However, we assume that the operation can be described by a dynamic system, taking inputs, denoted $u:[0,T]\to\mathbb{R}^p$, and giving outputs, denoted $y:[0,T]\to\mathbb{R}^q$, that we assume will be available as measurements in real time during the operation. At any given time, one of m distinct faults may arise, influencing the relationship between inputs and outputs. The operation is precisely defined so that a numerical simulator incorporating the potential faults can be built and used for planning prior to performing the operation in practice. Given a sequence of inputs, $\{u\}_{i=1}^n$ (for some arbitrary n), the type of fault (if any), an r-dimensional column-vector characterizing the fault, $d \in [-1,1]^r$, and an s-dimensional vector of (physical) system parameters $\theta \in [-1, 1]^s$, the simulator computes the corresponding sequence of outputs, $\{y\}_{i=1}^n$. We will denote this simulation as S_i , where the index $i \in \{0, 1, ..., m\}$ identifies the type of fault, with i = 0 corresponding to the fault-free operation. In other words, we have

$$\{y\}_{i=1}^{n} = S_{i}(\{u\}_{i=1}^{n}, d, \theta), i \in \{0, 1, ..., m\}.$$
 (1)

 θ can represent system parameters that are expected to change during operation, or whose inclusion in training can elevate the generalization performance of the DNN through the mechanism of MTL. Using data produced by the simulator, we aim to train a DNN so that it can be used in real time during the actual operation to detect a fault happening and yield an alarm with the type of fault and its characterizing vector d. (see Figure 1 for the proposed work flow). Denoting the neural network as f, we suggest the input-output structure

$$(\check{L}, \check{D}) = f(\{u\}_{i=1}^n, \{y\}_{i=1}^n, \theta)$$
 (2)

where $\check{L} \in \mathbb{R}^{m+1}$ and $\check{D} \in \mathbb{R}^{r \times (m+1)}$. For fault detection, define the one-hot labeling vectors $L_i = [l_0,...,l_m]$ where $l_j = 1$ for j = i and $l_j = 0$ for $j \neq i$,

and let \hat{L} equal the L_i , $i \in \{0,...,m\}$ that is most similar to \check{L} . The corresponding estimate of the diagnostics is then given by $\hat{d} = \check{D}\hat{L}$. We suggest Algorithm 1 for generating data for training and testing.

Algorithm 1: Data Generation.

Result: Datasets X and Y filled with input-output samples

Initialize datasets X and Y as empty;

while number of samples not reached do

Select i randomly from $\{0, \ldots, m\}$;

Select $\{u\}_{i=1}^n$ randomly from a class of admissible input signals;

Select d randomly from $[-1,1]^r$;

Select θ randomly from $[-1,1]^s$;

Compute $\{y\}_{i=1}^n = S_i(\{u\}_{i=1}^n, d, \theta)$;

Add $\{u\}_{i=1}^n, \{y\}_{i=1}^n, \theta$ to dataset X, and L_i, dL_i to dataset Y;

end

Let the data sets X,Y produced by Algorithm 1 contain N samples $(\{u\}_{i=1}^n, \{y\}_{i=1}^n, \theta)_j, (L_j, D_j), j \in \{1,...,N\}$. Invoking the NN (2) for each sample in X produces the predictions $\check{L}_j, \check{D}_j, j \in \{1,...,N\}$. The loss used for training is

$$\mathcal{L} = \underbrace{\mathcal{L}_{fd}}_{\text{fault detection}} + \underbrace{\mathcal{L}_d}_{\text{diagnosis}} \tag{3}$$

where

$$\mathcal{L}_{fd} = -\frac{1}{N} \sum_{j=1}^{N} L_j \cdot \log \check{L}_j \tag{4}$$

and

$$\mathcal{L}_{d} = \frac{1}{N} \sum_{i=1}^{N} L_{j} W ||(D_{j} - \check{D}_{j}) L_{j}||^{2}.$$
 (5)

 $W = [w_0, w_1, ..., w_m]^T$ is a vector of weights.

In the above, we have for notational simplicity ignored the fact that the diagnostics, d, may have dimension less than r for some faults (and dimension 0 for the fault-free case). This is handled in the implementation by masking out irrelevant components of d during training and testing.

At every timestep, t, the sequences of inputs, outputs, and parameters, $\{u\}_{i=t-n+1}^t, \{y\}_{i=t-n+1}^t$, and $\theta(t)$, from the operation can be fed to the pre-trained neural net to provide fault detection and diagnostics in real time, that is

$$(\check{L}(t), \check{D}(t)) = f(\{u\}_{i=t-n+1}^t, \{y\}_{i=t-n+1}^t, \theta(t))$$
 (6)

$$\hat{L}(t) = \underset{L_i, i \in \{0, \dots, m\}}{\arg \max} L_i \cdot \log \check{L}(t)$$
 (7)

$$\hat{d}(t) = \check{D}(t)\hat{L}(t) \tag{8}$$

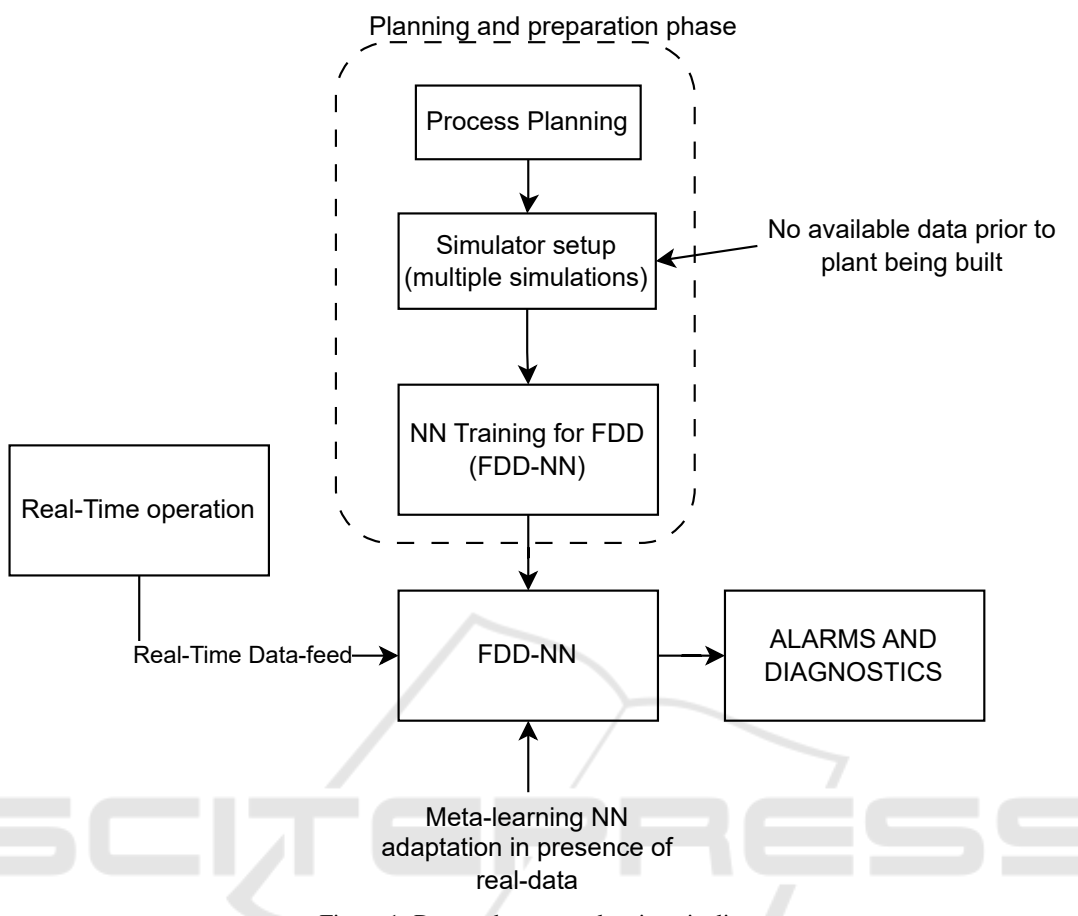


Figure 1: Data and process-planning pipeline.

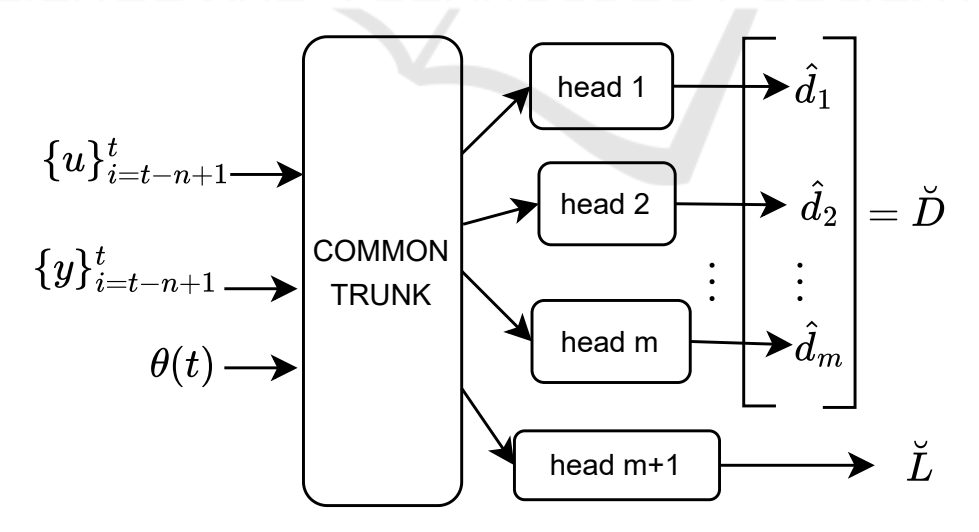


Figure 2: Depiction of a Multi-head Neural Network. Each one of the "heads" corresponds to a separate Fault with the last one corresponding to the detection task. Nomenclature of this figure corresponds to equations (6) - (8). The input θ represents process parameters for which the dataseries are produced. This is an input that is relevant when the training data are produced by different system parameters.

This FDD scheme is depicted in Figure 2. The MTL architectures tested for this work belong to the Hard Parameter Sharing architecture (Yu et al., 2024), meaning that the tasks share a subset of parameters and utilize a subset of specialized parameters which are not shared with the other tasks. Figure 2 offers a general depiction of such an architecture. Specifically, we compared the generalization performance between two similar architectures: Fully Connected Multi-task NN (FCN-MTL-NN) and Multi-head NN (MH-NN). The latter terminology is not consistent in the literature (Yu et al., 2024). In this work, we use this terminology when referring to a NN that uses separate DNNs for each head, whereas a Fully Connected Multi-task NN the heads are simply the last activation function of the final linear operation of the output layer. The consideration of certain process parameters θ is important for cases during which the system parameters change during operation. Instead of training multiple separate DNNs, we leverage the context-sensitive MTL architecture (Silver et al., 2008) for the system parameters and rely on a larger, more generalized DNN. In this architecture, a taskindicator (in this case, the system parameter vector θ) is propagated in the DNN from the input. In addition, more context-sensitive parameters may help achieve a higher generalization performance, which we opt to leverage in future work.

3 APPLICATION TO DRILLING

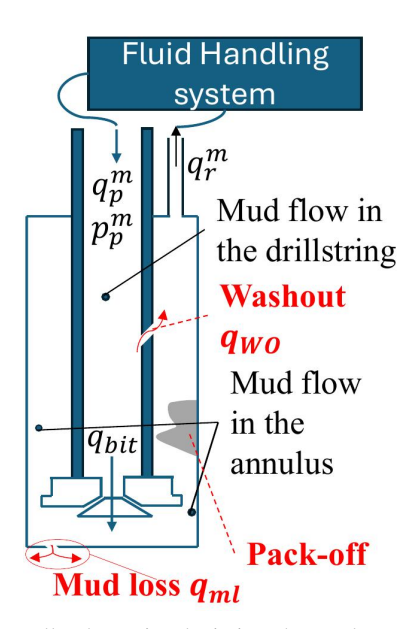
Figure 3a illustrates the drilling process. Measured quantities are indicated with the superscript m, while faults are highlighted in red. Drilling fluid, or "mud," is pumped through the drill string to the drill bit and then returns through the annulus to the Fluid Handling System (FHS), where it is cleaned and recirculated into the well. The pump rate q_p serves as the process input $(u(t) = q_p(t))$, while the pump pressure p_p and return flow q_r are the outputs $(y(t) = [p_p(t), q_r(t)])$. The relationship between input and output varies depending on whether a fault is present. The FHS is assumed to be open to the atmosphere on the annulus side, meaning that the pressure at that boundary is fixed at 1 bar. Managed Pressure Drilling (MPD) can be easily integrated as long as the pressure at the inlet of the MPD choke and the flow rate of the backpressure pump are measured. Washout occurs when fluid bypasses the normal flow path due to a crack or hole in the drill string, causing a shortcut from the drill string to the annulus. Its diagnostics include the crack location and size, represented as z_{wo} and C_{wo} . Mud loss happens when drilling fluid leaks from the well into

Table 1: Training parameters.

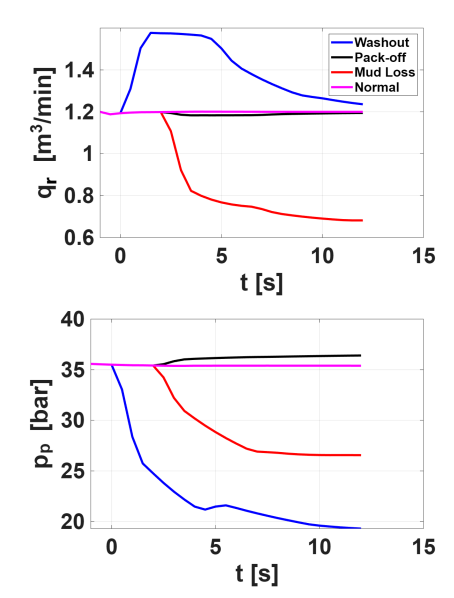
Parameter	Value
Batch type	Mini batch (size=400)
Number of sam-	{Washout: 8000, Packoff:
pled trajectories	8000 , Mud loss: 8000 }
Layer structure	$NN_{\text{head}} =$
for head	[80, 80, 80, 80, 80, 80, 2]
MH-NN struc-	[75, 1699, 1699, 1699,
ture	NN_{head} , NN_{head} , NN_{head} ,
	[80, 80, 80, 80, 80, 80, 4]]
FC-NN struc-	[75, 1272, 1272, 1272,
ture	1272, 1272, 12]
Number of	MH-NN: 6580134, FC-NN:
trainable pa-	6588972
rameters	
Activation func-	GELU (and SoftMax for the
tions	categorization output)
Loss function	Diagnosis: MSE, Detection:
	Cross Entropy
Regularization	L2 (0.01)
Optimizer	AdamW $(0.9, 0.9)$
	(Loshchilov and Hutter,
	2017)
Hardware	NVIDIA RTX A2000 Lap-
	top GPU (cuda) with Py-
	Torch

the reservoir. The key diagnostics for mud loss are the reservoir pressure and the mud-loss coefficient, denoted as p_r and k_I respectively. Pack-off refers to the partial or complete blockage of recirculation flow, often caused by inadequate hole cleaning, which allows cuttings to accumulate in the well. The key diagnostic for pack-off is the size coefficient linked to the pressure-drop across the blockage denoted by C_{po} . See equations (10) - (12) in the Appendix for details of the fault modeling.

The task of constructing an oil well constitutes a unique operation of the sort introduced in Section 2. The well is planned in detail before the operation, facilitating the setup of a simulator of the operation. In this work, we base the simulator on a mathematical description of the pressure and flow in the drill string and annulus in the form of a hyperbolic partial differential equation. The details of the model are given in the Appendix. For a constant pump rate of $q_p(t) = 1200$ [l/min], Figure 3b shows the return flow and pump pressure computed by the simulator for carefully selected examples of the three faults of interest. Notice that the pump pressure and return rate stay constant in the fault-free case (magenta lines). In the case of washout (blue lines), the return rate suddenly increases due to the short-cut suddenly created by the crack in the pipe. It quickly returns to



(a) Well schematic, depicting the Faults considered for this work. Figure from (Gkionis et al., 2025).



(b) Simulated trajectories from the Partial Differential Equations describing the system (see Appendix), showcasing the different behavior induced by the occurrence of different Faults.

Figure 3: Well schematic (left) and signatures of the different Faults (right).

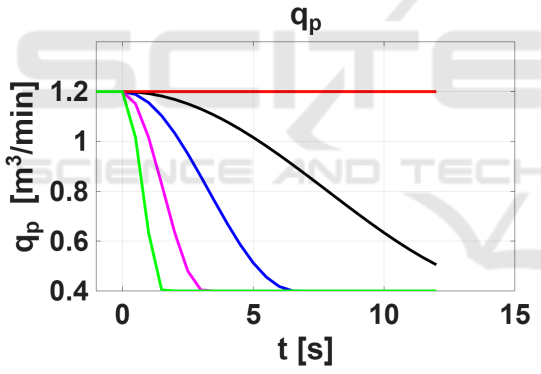


Figure 4: Different q_p trajectories. Each different color corresponds to a different set of A and γ of Equation (9). Blue: [0.8, 0.47], black: [0.8, 0.2], red: [0.8, 0], purple: [0.8, 1], green: [0.8, 02].

the original value of the pump flow, though, as mass balance is enforced. Due to the short-cut, the flow experiences less frictional pressure loss, and the required pump pressure to circulate therefore decreases. In the case of mud loss (red lines), the return flow decreases and stays low because mud is permanently lost to the reservoir. Less fluid therefore circulates, requiring a lower pump pressure. In the pack-off case (black lines), the flow stays relatively constant (since no mud is lost), while the frictional pressure loss increases due to the restriction pack-off causes, requiring a higher pump pressure to circulate. The pressure and flow signatures of the faults show quite distinct

features that can easily be identified by visual inspection. The purpose of the neural network, however, is to detect as early as possible less obvious faults that may evolve into serious problems for the operation if not counteracted.

Data for training and testing is produced according to Algorithm 1. In the algorithm, a set to draw admissible input signals from is defined by

$$q_p(t) = \frac{A_j}{2} \left(\cos \left(\max \left\{ 0, \min \left\{ \gamma_j t, \pi \right\} \right\} \right) + 1 \right) \quad (9)$$

where the parameters A_j , γ_j are uniformly sampled from [0.2, 1.0] and $[0, 2\pi/T_{\rm lim}]$ respectively. This corresponds to ramping the pump down from a rate governed by A_j at a slope governed by γ_j , which are likely operations of the pump in practice. Examples of this are shown in Figure 4.

As it has been already mentioned, this work focuses on performing accurate *Diagnosis* in the Drilling application. It is assumed that the faults do not occur simultaneously and that the system is operating in steady-state up until a fault occurrence.

As a first step to assessing the robustness of the FDD scheme, we generate data using simulations for uniformly sampled values of the depth of the well L in the range [2000m, 4000m]. The architecture used for this addition is the one shown in Figure 2 with $\theta(t)$ equal to L(t) normalized to the interval [-1,1]. L clearly varies slowly compared to the dynamics of pressure and flow.

Table 2: Detection accuracy for the different faults.

-	Washout	Mud Loss	Pack-off
Fixed depth (3000m)	99.5%	100%	100%
Variable depth	99.7%	100%	100%

The motivation for using the specific time window of T = 12s and sampling time of $\Delta t = 0.5s$ is linked to the dynamics of the system. The nature of the pressure waves in this system is such that there will be a delay until the effects of a fault become apparent at the topside boundary. This can be verified via visual inspection of the delays for the first signal changes to occur Figure 3b).

RESULTS AND DISCUSSION

The hyperparameters of the training algorithm are provided in Table 1. Figures 5a and 5b show the scatterplots for the predictions on the diagnostic variables for fixed (first row) and randomized well depth (second row) for Washout and Mud Loss respectively and Figure 6 shows the same information for Pack-off. In this section, we present the results of applying the test data to the trained network. The performance of classification of the type of fault (i.e. fault detection) is summarized in Table 2 for the cases of fixed and variable well depth. It can be observed that Diagnosis is accurate when the well depth is fixed and exhibits 5. In spite of the established theory (Zhang et al., moderate robustness with respect to the well depth parameter. The MH-NN trained on data a fixed well depth of 3000 m exhibits quite higher accuracy using the same number of training datapoints (8000).

- 1. The MH-NN (Figure 2) generalizes equally well with a FCN that has multiple outputs. The depth of the NN was crucial to the results; a shallow NN (with the same number of trainable parameters) resulted in gradient vanishing, as well as with depth quite larger than the one used for this work.
- 2. The NN trained for trajectories with randomly sampled well depths exhibited unsurprisingly lower accuracy for Fault Diagnosis. Enlarging the training dataset and/or the NN would improve the prediction accuracy. In addition, utilization of useful biases linked to the effect of the well depth in the dynamics, and application of meta-learning in already trained NNs can result in improvement of the NN's generalization performance.
- 3. The outliers in Figure 5a and Figure 5b are not surprising. C_{wo} becomes difficult to correctly diagnose when the washout occurs close to the bit, since then the flow through the crack and the

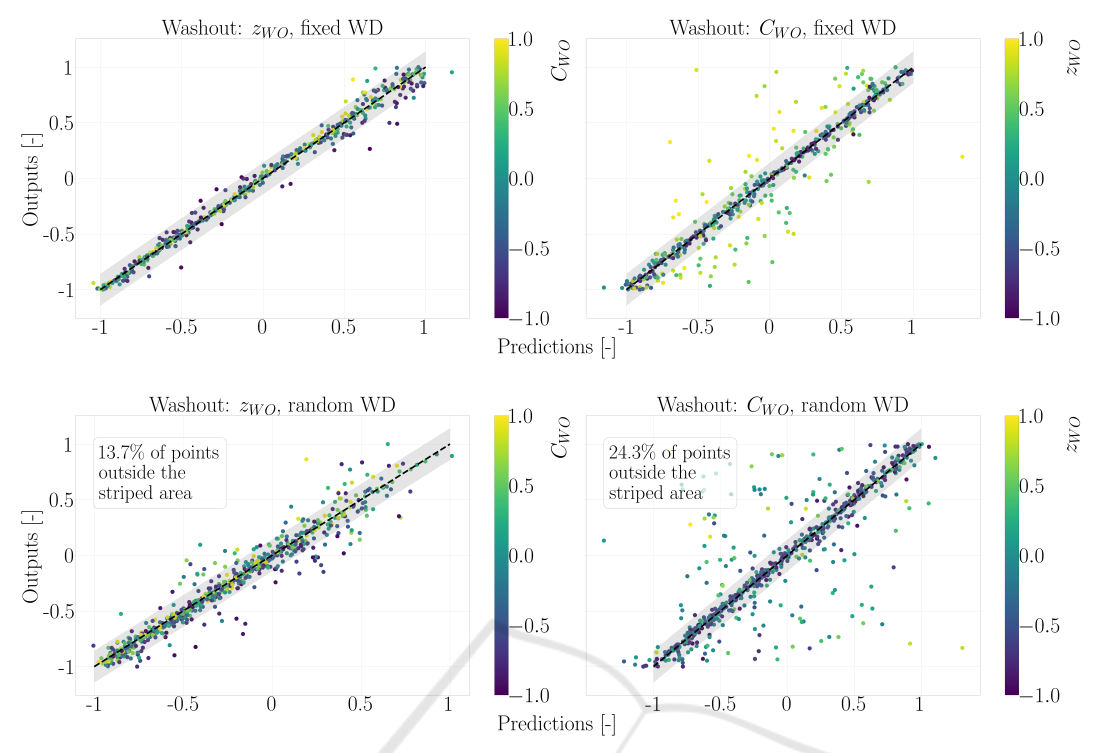
flow through the bit are indistinguishable from the top-side, several kilometers away. Diagnosing z_{wo} for small washouts is also quite difficult because accurate localization is sensitive to the difference between the pump rate and the rate of flow through the bit. It is this difference that causes a change in the pump pressure which can be detected top-side. When it comes to mud loss (Figure 5b, the reservoir pressure p_r is generally well predicted, while the index k_I is occasionally quite wrong. We do not have a clear explanation for this behavior, but in practice, it is more important to obtain an accurate estimate of the reservoir pressure because then the down-hole pressure one needs to aim for in order to stop the loss is known. The down-hole pressure can be lowered to some extent by ramping down the pump, and to a larger extent by changing the mud weight.

- The high prediction quality (for fixed well depth), achieved without weight scheduling or special regularization (Mao et al., 2024), suggests that task domination (Senushkin et al., 2023) may be absent in the studied datasets.
- 2016) that overparameterization generates implicit regularization, the multi-head architecture still required weight decay in order to generalize in an acceptable level.

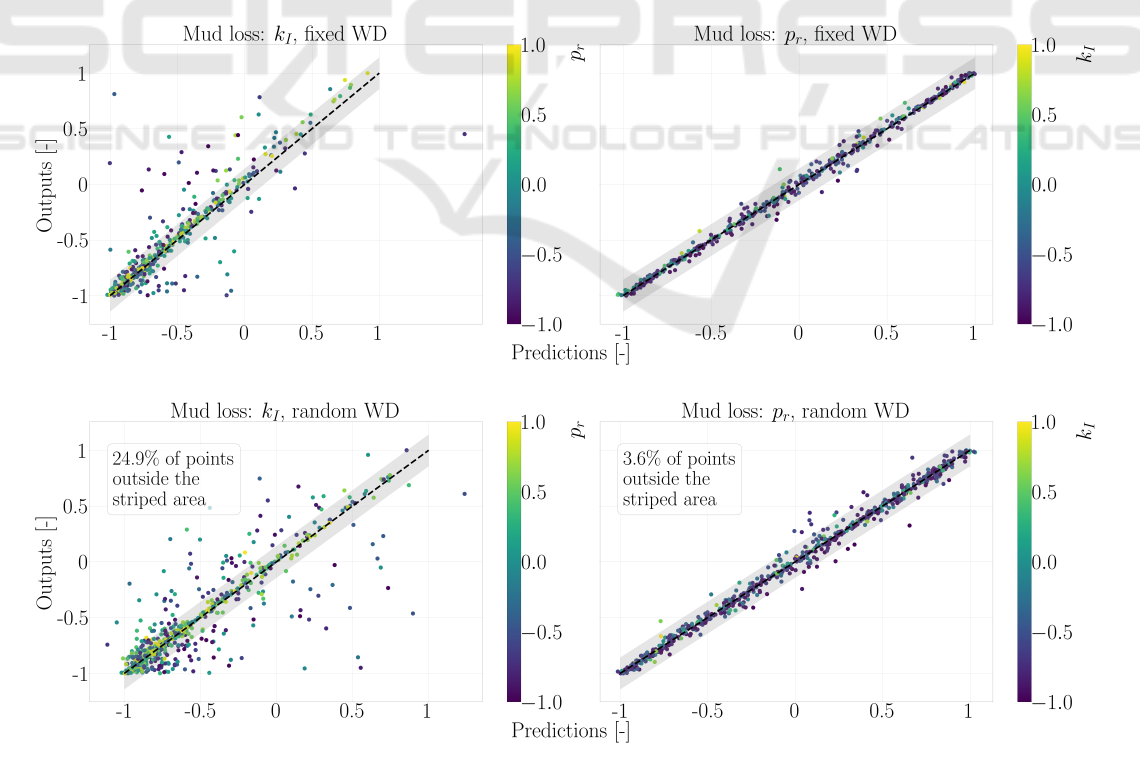
CONCLUSIONS AND FUTURE WORK

In this work, a MTL-NN was successfully trained to perform accurate Fault Diagnosis through deployment of a single multi-head NN trained on simulated time-series trajectories. It constitutes a preliminary step towards using generalized NNs that predict accurately for wider spectrum of faults and well parameters, as well as parameters of the fault-free process. Our NN generalizes to different well depths with significant room for improvement. In addition, the requirement for an increased network depth is typically suggestive of the presence of hierarchical complexity in the dataset.

An immediate idea for extending this work would be to improve the data-efficiency of MTL that per-

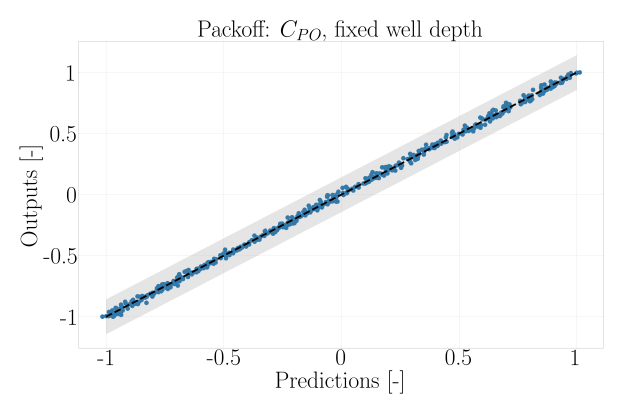


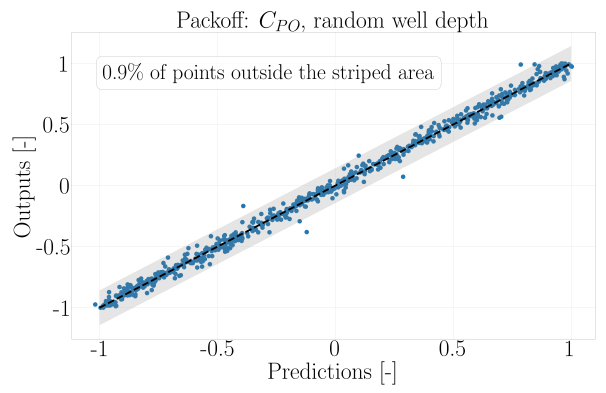
(a) Scatterplots of Washout diagnostics on test data, using the MH-NN for fixed Well Depth and random Well Depth



(b) Scatterplots of Mud Loss diagnostics on test data, using the MH-NN for fixed Well Depth and random Well Depth

Figure 5: Scatterplots for the faults. The values are normalized in [-1, 1]. The x-axis represents the network's prediction and the y-axis represents the actual values for the diagnostics.





(a) Scatterplot of Pack-off diagnostics on test data, using the MH-NN.

(b) Scatterplot using MH-NN trained on randomized well depth data.

Figure 6: Scatterplots for the faults. Values normalized in [-1,1]. The x-axis represents the network's prediction and the y-axis represents the actual values for the diagnostics.

forms FDD with the same NN for different well depths (as well as other well characteristics, such as the well geometry, varying drill string cross-sections, and drilling fluid), given the satisfactory accuracy that we have achieved using the same NN that was trained for data generated using a fixed well depth.

In addition to this, considering more well parameters would bring about higher generalization performance and creating a more general NN that can then be used to finely update a subset of the Network parameters for unseen wells based on *meta-learning* (Hospedales et al., 2020) and few-shot learning (Zou and Karniadakis, 2023). What is more, it is speculated that the consideration of multiple sources of parameter uncertainty will render detection of the faults challenging, since it is expected that there will be very similar curves corresponding to different faults and different well parameters. This possibility gives rise to the requirement for developing and training NNs that incorporate uncertainty (He and Jiang, 2023). Further work on rendering the scheme more robust and realistic via incorporating uncertainty in the data and the system parameters would be to include colored noise in the input data.

The most important limitation of our work is, admittedly, the complete reliance on simulated data for NN training. The motivations for this are as follows.

• Preliminary investigation of the feasibility of performing FDD given the known dynamics of a problem. Up to our knowledge, this is the first work that tackles the inverse problem of identifying fault parameters in drilling for multiple faults and utilizing only topside measurements. Therefore, a first step towards FDD is to investigate its feasibilty with synthetic data.

• Insufficient number of real process data. As explained in Section 1, real drilling data during faulty operations are not expected to be sufficient for DNN training. This is true for other applications as well (for example, in (Tercan et al., 2018) and (Weber et al., 2020)). Tackling this challenge requires utilization of methods that transfer knowledge from simulations to real data.

Since the synthetic data bear similarities with the real drilling data, the knowledge encoded in DNNs trained with simulation data may be exploited such that the DNN adapts to sparse real process data. The techniques that facilitate this adaptation are Transfer Learning and Meta-Learning (Hospedales et al., 2020), (Ranaweera and Mahmoud, 2021). Numerous industrial applications which leverage Transfer Learning exist in literature, many of which are detailed in (Yan et al., 2023). For example, the authors in (Tercan et al., 2018) tackle the problem of low availability of real industrial data for training in injection mold methods by training a DNN with simulated data and then introduce new NN parameters for training on real data while keeping the simulation-trained ones frozen, or use the already trained values of the weights as initial values for training with the limited real training data. The authors in (Weber et al., 2020) train base DNN models to detect room occupancy using synthetic data from room occupancy simulations and physical simulations. These base models are subsequently updated through a transfer step to adapt to the limited (and more expensive to sample) real data. Up to our knowledge, there is not any research work that applies Transfer Learning and/or Meta-Learning to bridge the gap between simulated and real data in drilling applications.

Last but not least, to enhance the practicability of the developed algorithm, extensive testing with stateof-the-art drilling simulators can be conducted. Such simulators (for example, OpenLAB from (Gravdal et al., 2021)) can model faults which cannot are governed by much more complicated dynamics, such as Gas-Kick (Sun et al., 2018).

REFERENCES

- Alzubaidi, L., Zhang, J., Humaidi, A. J., Al-dujaili, A., Duan, Y., Al-Shamma, O., Santamaría, J. I., Fadhel, M. A., Al-Amidie, M., and Farhan, L. (2021). Review of deep learning: concepts, cnn architectures, challenges, applications, future directions. *Journal of Big Data*, 8.
- Amyar, A., Modzelewski, R., and Ruan, S. (2020). Multitask deep learning based ct imaging analysis for covid-19: Classification and segmentation. *medRxiv*.
- Caruana, R. (1997). Multitask learning. *Machine Learning*, 28:41–75.
- Gkionis, M., Wilhelmsen, N. C. A., and Aamo, O. M. (2025). Fault diagnosis for drilling using a multitask physics-informed neural network. In *Proceedings of the 14th IFAC Symposium on Dynamics and Control of Process Systems, including Biosystems (DYCOPS)*. To appear.
- Gravdal, J. E., Sui, D., Nagy, A. P., Saadallah, N., and Ewald, R. (2021). A hybrid test environment for verification of drilling automation systems.
- Guo, S., Zhang, B., Yang, T., Lyu, D., and Gao, W. (2020). Multitask convolutional neural network with information fusion for bearing fault diagnosis and localization. *IEEE Trans. Ind. Electron.*, 67(9):8005–8015.
- He, W. and Jiang, Z. (2023). A survey on uncertainty quantification methods for deep learning.
- Hospedales, T. M., Antoniou, A., Micaelli, P., and Storkey, A. J. (2020). Meta-learning in neural networks: A survey. *IEEE Transactions on Pattern Analysis and Machine Intelligence*, 44:5149–5169.
- Isermann, R. (2006). Fault-diagnosis systems: an introduction from fault detection to fault tolerance.
- Jan, A., Mahfoudh, F., Draškovic, G., Jeong, C., and Yu, Y. (2022). Multitasking physics-informed neural network for drillstring washout detection. 2022(1).
- Jeong, C., Yu, Y., Mansour, D., Vesslinov, V., and Meehan, R. (2020). A physics model embedded hybrid deep neural network for drillstring washout detection.
- Jiang, H., hui Liu, G., Li, J., Zhang, T., and Wang, C. (2020). A realtime drilling risks monitoring method integrating wellbore hydraulics model and streaming-data-driven model parameter inversion algorithm. *Journal of Natural Gas Science and Engi*neering, page 103702.
- Lin, Z., Zhao, Z., Zhang, Z., Baoxing, H., and Yuan, J. (2021). To learn effective features: Understanding the task-specific adaptation of {maml}.
- Liu, Z., Wang, H., Liu, J., Qin, Y., and Peng, D. (2021).
 Multitask learning based on lightweight 1DCNN for

- fault diagnosis of wheelset bearings. *IEEE Trans. Instrum. Meas.*, 70:1–11.
- Loshchilov, I. and Hutter, F. (2017). Decoupled weight decay regularization. In *International Conference on Learning Representations*.
- Mao, D., Chen, Y., Wu, Y., Gilles, M., and Wong, A. (2024). Robust analysis of multi-task learning efficiency: New benchmarks on light-weighed backbones and effective measurement of multi-task learning challenges by feature disentanglement.
- Qiu, S., Cui, X., Ping, Z., Shan, N., Li, Z., Bao, X., and Xu, X. Y. (2023). Deep learning techniques in intelligent fault diagnosis and prognosis for industrial systems: A review. Sensors (Basel, Switzerland), 23.
- Raissi, M., Perdikaris, P., and Karniadakis, G. E. (2019). Physics-informed neural networks: A deep learning framework for solving forward and inverse problems involving nonlinear partial differential equations. *J. Comput. Phys.*, 378:686–707.
- Ranaweera, M. and Mahmoud, Q. H. (2021). Virtual to realworld transfer learning: A systematic review. *Elec*tronics.
- Senushkin, D., Patakin, N., Kuznetsov, A., and Konushin, A. (2023). Independent component alignment for multi-task learning. 2023 IEEE/CVF Conference on Computer Vision and Pattern Recognition (CVPR), pages 20083–20093.
- Silver, D. L., Poirier, R., and Currie, D. (2008). Inductive transfer with context-sensitive neural networks. *Machine Learning*, 73:313–336.
- Sun, X., Sun, B., Zhang, S., Wang, Z., Gao, Y., and Li, H. (2018). A new pattern recognition model for gas kick diagnosis in deepwater drilling. *Journal of Petroleum Science and Engineering*.
- Tercan, H., Guajardo, A., Heinisch, J., Thiele, T., Hopmann, C., and Meisen, T. (2018). Transfer-learning: Bridging the gap between real and simulation data for machine learning in injection molding. *Procedia CIRP*, 72:185–190.
- Venkatasubramanian, V., Rengaswamy, R., Kavuri, S. N., and Yin, K. K. (2003). A review of process fault detection and diagnosis: Part iii: Process history based methods. *Comput. Chem. Eng.*, 27:327–346.
- Wang, H., Liu, Z., Peng, D., Yang, M., and Qin, Y. (2021a). Feature-level attention-guided multitask cnn for fault diagnosis and working conditions identification of rolling bearing. IEEE Trans. Neural Netw. Learn. Syst.
- Wang, H., Liu, Z., Peng, D., Yang, M., and Qin, Y. (2022). Feature-level attention-guided multitask CNN for fault diagnosis and working conditions identification of rolling bearing. *IEEE Trans. Neural Netw. Learn. Syst.*, 33(9):4757–4769.
- Wang, H., Zhao, H., and Li, B. (2021b). Bridging multi-task learning and meta-learning: Towards efficient training and effective adaptation. *ArXiv*, abs/2106.09017.
- Weber, M., Doblander, C., and Mandl, P. (2020). Towards the detection of building occupancy with synthetic environmental data. *ArXiv*, abs/2010.04209.
- Willersrud, A., Blanke, M., Imsland, L. S., and Pavlov, A. K. (2015). Fault diagnosis of downhole drilling in-

cidents using adaptive observers and statistical change detection. *Journal of Process Control*, 30:90–103.

Yan, P., Abdulkadir, A., Luley, P.-P., Rosenthal, M., Schatte, G. A., Grewe, B. F., and Stadelmann, T. (2023). A comprehensive survey of deep transfer learning for anomaly detection in industrial time series: Methods, applications, and directions. *IEEE Access*, 12:3768– 3789.

Yu, J., Dai, Y., Liu, X., Huang, J., Shen, Y., Zhang, K., Zhou, R., Adhikarla, E., Ye, W., Liu, Y., Kong, Z., Zhang, K., Yin, Y., Namboodiri, V., Davison, B. D., Moore, J. H., and Chen, Y. (2024). Unleashing the power of multi-task learning: A comprehensive survey spanning traditional, deep, and pretrained foundation model eras. *ArXiv*, abs/2404.18961.

Zhang, C., Bengio, S., Hardt, M., Recht, B., and Vinyals, O. (2016). Understanding deep learning requires rethinking generalization. *ArXiv*, abs/1611.03530.

Zhang, Q. (2000). A new residual generation and evaluation method for detection and isolation of faults in non-linear systems. *International Journal of Adaptive Control and Signal Processing*, 14:759–773.

Zou, Z. and Karniadakis, G. E. (2023). L-hydra: Multihead physics-informed neural networks. ArXiv, abs/2301.02152.

APPENDIX

In this section, the partial differential equations describing the drilling dynamics, including the potential faults, are given. The state variables are pressure in the drill string $(p_d(z,t))$, pressure in the annulus $(p_a(z,t))$, volumetric flow in the drill string $(q_d(z,t))$, and volumetric flow in the annulus $(q_a(z,t))$. $q_p(t)$ is the applied pump rate (volumetric flow) into the drill string, while p_0 is the atmospheric pressure at the outlet of the annulus. The well length is L, so that $z \in [0,L]$ and z=0 is at the top of the well. For simplicity, a vertical well with spatially invariant cross section is assumed.

The nomenclature with the respective values is given in Table 3 used in the simulations of Section 3.

The three faults that we consider are modeled as follows. The washout flow is given by

$$q_{wo}(t) = C_{wo} \sqrt{p_d(z_{wo}, t) - p_a(z_{wo}, t)},$$
 (10)

the mud loss flow is given by

$$q_{ml}(t) = k_I(p_a(L,t) - p_r),$$
 (11)

and the pack-off pressure loss is given by

$$p_{po}(t) = \frac{A_a}{C_{po}^2} q_a^2(L, t). \tag{12}$$

We have opted to diagnose Pack-off by considering that it takes place at the bottom of the well.

Denoting $\partial_x y \triangleq \frac{\partial y}{\partial x}$ and the Dirac delta function by $\delta(z)$, we have the dynamics

$$\partial_t p_d(z,t) = -\frac{\beta}{A_d} (\partial_z q_d(z,t) + \delta(z - z_{wo}) q_{wo}) \quad (13)$$

$$\partial_t q_d(z,t) = -\frac{A_d}{\rho} \partial_z p_d(z,t) - f_d(q_d(z,t)) + A_d g \tag{14}$$

$$\partial_t p_a(z,t) = -\frac{\beta}{A_a} (\partial_z q_a(z,t) - \delta(z - z_{wo}) q_{wo}) \quad (15)$$

$$\partial_t q_a(z,t) = -\frac{A_a}{\rho} \partial_z p_a(z,t) - f_a(q_a(z,t)) + A_a g \tag{16}$$

$$+\delta(z-L)p_{po}$$

with boundary conditions

$$q_d(0,t) = q_p(t) \tag{17}$$

$$p_a(0,t) = p_0 (18)$$

$$p_d(L,t) = p_a(L,t) + \frac{1}{C_{bit}^2} q_d^2(L,t)$$
 (19)

$$q_a(L,t) = -q_d(L,t) + k_I \max\{p_a(L,t) - p_r, 0\}.$$
(20)

In practice, only the pump rate $q_p(t)$, pump pressure $p_p(t) = p_d(0,t)$ and return flow $q_r(t) = -q_a(0,t)$ are commonly measured. The diagnostics are normalized to the interval [-1,1]. For example, let $C_{wo} \in [C_{wo,min}, C_{wo,max}]$. Then, the normalized diagnostic is given by

$$d = 2\frac{C_{wo} - C_{wo,min}}{C_{wo,max} - C_{wo,min}} - 1.$$
 (21)

The simulator implements the dynamics using first order finite differences on a staggered grid.

From Table 3, the friction coefficient quantifies the pressure drop along a pipe (drillstring and annulus in our case) per unit length for a fluid flow of $1 \ m^3/min$ across the pipe. The formula is given below.

$$f_{d/a} \triangleq \Delta p_{d/a} \frac{A_{d/a}}{\rho} \tag{22}$$

 $\Delta p_{d/a}$ was selected as 5 $bar/km/(m^3/min)^2$ for the drillstring and 3 $bar/km/(m^3/min)^2$ for the annulus.

The bit valve coefficient expresses the pressure drop over the bit at a given flow. We assumed a 10 *bar* pressure drop at 1.5 m^3/min flow. The valve coefficient formula is given below.

$$C_{bit} \triangleq \frac{q}{\sqrt{\Delta p_{bit}/\rho}} \tag{23}$$

Table 3: List of symbols in the PDE equations with their respective values (if they correspond to a fixed parameter).

Symbol	Description	Value
β	Bulk modulus of the drilling fluid	$1.8 \times 10^4 \text{ bar}$
ρ	Density of the drilling fluid	1000 kg/m^3
g	Acceleration of gravity	9.81 m/s^2
$A_{d/a}$	Cross-sectional area of drill string/annulus	[127,366] cm ²
$f_{d/a}$	Drillstring and annulus friction coefficients	$[13.7,65.9] 1/m^3$
C_{bit}	Bit valve coefficient	$0.0053 \text{ m}^3/\text{s/bar}^{0.5}$
C_{wo}	Washout size coefficient (diagnostic)	
z_{wo}	Washout location (diagnostic)	_
C_{po}	Pack-off size coefficient (diagnostic)	_
z_{po}	Pack-off location (diagnostic)	_
\dot{k}_I	Flow coefficient for mud-loss (diagnostic)	-
p_r	Reservoir pressure (diagnostic)	_

